Eur. J. Mech. B/Fluids 18 (1999) 1085–1101

Stability of plane-parallel vibrational flow in a two-layer system

M.V. Khenner [a], D.V. Lyubimov [a], T.S. Belozerova [a], B. Roux [b,*]

[a] *Perm State University, 15 Bukirev str., 614600 Perm, Russia*
[b] *IRPHE-IMT, UMR 6594, 13451 Marseille cedex 20, France*

(Received 10 November 1997; revised 21 December 1998; accepted 24 September 1999)

Abstract – The stability of the interface separating two immiscible incompressible fluids of different densities and viscosities is considered in the case of fluids filling a cavity which performs horizontal harmonic oscillations. There exists a simple basic state which corresponds to the unperturbed interface and plane-parallel unsteady counter flows; the properties of this state are examined. A linear stability problem for the interface is formulated and solved for both (a) inviscid and (b) viscous fluids. A transformation is found which reduces the linear stability problem under the inviscid approximation to the Mathieu equation. The parametric resonant regions of instability associated with the intensification of capillary-gravity waves at the interface are examined and the results are compared to those found in the viscous case in a fully numerical investigation. © 1999 Éditions scientifiques et médicales Elsevier SAS

horizontal harmonic oscillation / inviscid fluid / viscous fluid

1. Introduction

Vibration is a factor of a significant influence on processes involving fluids (liquids or gases) with non-uniform density. In fact, a non-uniform inertial field (in the cavity frame) appears in such fluids subject to vibration, and can influence heat and mass transfers. The density non-uniformity might be caused by different factors, including (i) temperature and/or concentration gradients, (ii) presence of interfaces and/or free surfaces, (iii) presence of inclusions, etc. In the present paper, we consider an interface between two liquid layers subject to horizontal harmonic vibrations, of amplitude a and frequency ω.

It is known that vertical vibrations can lead both to the parametric excitation of waves at the interface and to the suppression of the Rayleigh–Taylor instability [1–4], while the effects due to horizontal vibrations have been studied less. In experimental works by Wolf [5] and Bezdeneznykh et al. [6] for a long horizontal reservoir filled with two immiscible viscous fluids, an interesting phenomenon was found at the interface: the horizontal vibrations lead to the formation of a steady relief. This formation mechanism has a threshold nature; it is noteworthy that such a wavy relief appears on the interface only if the densities of the two fluids are close enough, i.e. it does not appear for the liquid/gas interface (free surface). The interface is absolutely unstable if the heavier fluid occupies the upper layer; i.e. the horizontal vibration does not prevent the evolution of the Rayleigh–Taylor instability, in contrast to vertical vibration which under certain conditions suppresses its evolution. A theoretical description of this phenomenon was provided by Lyubimov and Cherepanov [7] within the framework of a high frequency (of the vibration) approximation and an averaging procedure; they found that a horizontal vibration leads to a quasi-equilibrium state, i.e. a state where the mean motion is absent but the interface oscillates with a small amplitude (of the order of magnitude of the cavity displacement) with respect to the steady relief. In particular, they found that the relief (in the case of a heavy fluid occupying the bottom

* Correspondence and reprints; broux@irphe.univ-mrs.fr

layer) with finite wavelength is not possible for any fluid layer thickness. In fact, a relief with finite wavelength arises only for considerably thick layers of height $h > [3\alpha/(g(\rho_1-\rho_2))]^{1/2}$, where α is the coefficient of surface tension, ρ_1 and ρ_2 are the densities of lower and upper layer, respectively; g is the gravity acceleration. In the approach [7], two parameters were assumed to be asymptotically small simultaneously: (i) the dimensionless thickness of the viscous skin-layers $\delta = h^{-1}\sqrt{\nu/\omega}$, ν being the kinematic viscosity and (ii) the dimensionless amplitude of the vibration $\varepsilon = a/h$. But in the limiting case $\varepsilon \to 0$, the possibility of the description of the parametric resonant effects is absent and only the basic instability mode (of Kelvin–Helmholtz type, for two counter flows) remains.

In the present investigation, the condition $\varepsilon \to 0$ is dropped and the vibration frequency is not assumed to be high, so the averaging method [7] could no longer be applied.

The instability of an interface between two time-dependent counter flows was considered in [8] for infinitely deep layers. This is a limiting case compared to the situation considered in the present paper. But, as will be shown in Section 3, for layers of finite thicknesses there arise qualitatively new phenomena which do not occur for infinitely deep layers. In addition, the study in [8] was carried out for inviscid liquids, while the influence of viscosity is analyzed in Section 4 of the present paper.

The contents of our paper are as follows. In Section 3, the resonant effects are studied in the case of $\delta \to 0$, i.e. when the thickness of the viscous skin-layer is much smaller than all the characteristic lengths. Alternatively, the period of the vibration is assumed to be small in comparison with the viscous damping time but comparable to the capillary-gravity time. The condition $\delta \to 0$ means that, in the equations of motion, the viscous terms are omitted, i.e. the problem is considered under the inviscid approximation.

In Section 4, the 2D linear stability problem is set up for viscous fluids. The problem of neutral stability is reduced to the analysis of two systems of first order ordinary differential equations (in space) for the disturbance amplitudes, with boundary conditions imposed on the rigid walls and on the interface. These boundary values problems (BVP's) are solved by using a numerical integration. The numerical results are presented in Section 5.

For readers interested in resonant surface waves, we can mention a study by Ockendon and Ockendon [9] which concerns a single layer with a free surface in a container subject to small amplitude oscillations, horizontal or vertical, and a more recent work by Ockendon and Ockendon [10] on multi-mode resonances in fluids (the sloshing of liquid in a horizontally oscillating, rectangular tank). The problem that we consider here is different. It concerns a two-layer system in a long cavity where oscillations generate a basic flow (plane-parallel unsteady counter flow) and we are interested in the stability of such a basic state.

2. Problem formulation

Let us consider the system of two immiscible, incompressible, liquids filling a rectangular cavity of length L and height h. In the state of rest the heavy liquid (of density ρ_1) occupies the bottom region of height h_1, and the light liquid (of density ρ_2)—the upper region of height h_2 ($h = h_1 + h_2$). We choose a Cartesian coordinate system in such a way that the x, y-axes lie in the horizontal plane, the z-axis is directed vertically, $z = 0$ corresponds to the unperturbed interface. Let the cavity perform a harmonic oscillation along the x-axis, with amplitude a and frequency ω, and let $\vec{\gamma}$ be the unit vector along the z-axis, and $\vec{j}$ along the vibration axis (*figure 1*).

The vibration of each vertical endwall generates a wave on the interface. This wave propagates from to the central part of the cavity; but, if the viscosities of the liquids are not too small, it is damped over relatively short distances from the endwall. For example, for transformer oil and glycerine in the earth's gravitational field and angular frequencies of the vibration of the order of magnitude 100 Hz, the damping length l_d is of the order

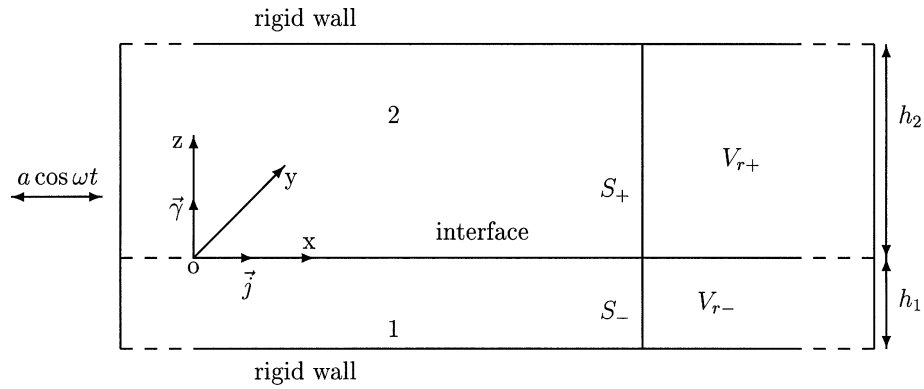

Figure 1. Configuration of the problem.

of magnitude of 1 mm. In the following, we consider a long enough cavity for which the condition $L \gg l_d$ is satisfied and we consider only the central part of this cavity, far away from the endwalls, where the interface waves generated near the endwalls are damped. Therefore in the basic state the interface will be considered as planar and horizontal.

However, the liquid in the central part of the cavity cannot stay at rest, and the velocities of the liquid motion in the bottom and upper layers must be different. Indeed, since the densities of both liquids are different, then the pressure gradients would be different if the velocities in both layers were equal. This would contradict the normal stress balance condition at the interface. The only exception might be the case of liquids which stay at rest in the laboratory reference frame, but such a situation is impossible due to the incompressibility condition. To prove this, let us consider the cross-section of the cavity by the vertical plane $S = S_- + S_+$, attached to the cavity (*figure 1*). Then, the liquid volume $V = V_{r-} + V_{r+}$ to the right (for example) of the cross-section is constant by virtue of the incompressibility. At the same time, the volume of each liquid cannot be constant because the interface is not at rest near the vertical endwalls; a time-dependent sloshing motion is generated there. This means that in the cavity frame, at each instant, there is an exact balance of the displaced volume of both liquids through S, i.e.

$$\forall x: \quad \int_{-h_1}^{\xi} v_{1x}\, dz = -\int_{\xi}^{h_2} v_{2x}\, dz, \tag{1}$$

where ξ is the vertical coordinate of the interface.

In summary, we expect that the sloshing motion generated near the vertical endwalls will induce a long range circulation in such a long cavity. The condition (1) must be satisfied for such a basic state. We assume that the interface waves associated to the sloshing motion near the endwalls do not penetrate into the central part of the cavity, due to viscous damping. According to the above discussion we will use the approximation of infinite horizontal layers.

As is obvious from (1), the basic flow is of counter-flow type, so we expect the Kelvin–Helmholtz instability, while the periodic character of the flow allows us to expect parametric resonance effects as well. The inviscid case is studied in Section 3, and the viscous case in Section 4.2.

In the cavity frame, time-dependent inertia forces should be accounted for, i.e.

$$-g\vec{\gamma} \to -g\vec{\gamma} + a\omega^2 \vec{j}\cos\omega t.$$

Thus, the full Navier–Stokes equations become

$$\frac{\partial \vec{v}_\beta}{\partial t} + (\vec{v}_\beta \nabla)\vec{v}_\beta = -\frac{1}{\rho_\beta}\nabla p_\beta + \nu_\beta \Delta \vec{v}_\beta - g\vec{\gamma} + a\omega^2 \vec{j}\cos\omega t \tag{2}$$

and the continuity equations for the two layers are

$$\operatorname{div} \vec{v}_\beta = 0, \tag{3}$$

where the subscript $\beta = 1, 2$ refers to the lower and upper layers, respectively, the other notation being conventional.

No-slip boundary conditions for the velocity are imposed on the rigid walls of the cavity:

$$\text{at } z = -h_1: \quad \vec{v}_1 = 0, \tag{4a}$$

$$\text{at } z = h_2: \quad \vec{v}_2 = 0, \tag{4b}$$

while on the interface $z = \xi(x, y, t)$, the following conditions are satisfied:

– stress balance

$$(p_1 - p_2)n_i = (\sigma_{ik}^{(1)} - \sigma_{ik}^{(2)})n_k + \alpha n_i \operatorname{div} \vec{n}; \tag{5}$$

– velocity continuity

$$\vec{v}_1 = \vec{v}_2; \tag{6}$$

– kinematic condition

$$\frac{\partial \xi}{\partial t} + (\vec{v}_1 \nabla)\xi = \vec{v}_1 \cdot \vec{\gamma}. \tag{7}$$

In (5)–(7), α is the surface tension coefficient, $\sigma_{ik}^{(\beta)}$ are the viscous stress tensors:

$$\sigma_{ik}^{(\beta)} = \frac{\partial v_{\beta,i}}{\partial x_k} + \frac{\partial v_{\beta,k}}{\partial x_i}.$$

The integral condition of balance of the displaced volume of both liquids is

$$\forall x: \quad \int_{-h_1}^{\xi} \vec{v}_1 \cdot \vec{j}\, dz + \int_{\xi}^{h_2} \vec{v}_2 \cdot \vec{j}\, dz = 0. \tag{8}$$

3. Inviscid approximation

After omitting the viscous term, the Navier–Stokes equations (2) become

$$\frac{\partial \vec{v}_\beta}{\partial t} + (\vec{v}_\beta \nabla)\vec{v}_\beta = -\frac{1}{\rho_\beta}\nabla p_\beta - g\vec{\gamma} + a\omega^2 \vec{j}\cos\omega t. \tag{9}$$

The continuity equations remain unaltered:

$$\operatorname{div} \vec{v}_\beta = 0. \tag{10}$$

The impermeability boundary conditions are imposed on the rigid walls instead of the no-slip conditions:

$$\text{at } z = -h_1: \quad \vec{v}_1 \cdot \vec{\gamma} = 0, \tag{11}$$

$$\text{at } z = h_2: \quad \vec{v}_2 \cdot \vec{\gamma} = 0. \tag{12}$$

At the interface $z = \xi(x, y, t)$ the following conditions are imposed:

– normal stress balance

$$p_1 - p_2 = \alpha \operatorname{div} \vec{n}; \tag{13}$$

– continuity of normal components of velocity

$$\vec{v}_1 \cdot \vec{n} = \vec{v}_2 \cdot \vec{n}; \tag{14}$$

– kinematic condition

$$\frac{\partial \xi}{\partial t} + (\vec{v}_1 \nabla)\xi = \vec{v}_1 \cdot \vec{\gamma}. \tag{15}$$

The condition (8) for the balance of the displaced volumes remains unaltered.

The problem (9)–(15), (8) admits a solution of the form

$$\vec{V}_\beta = U_\beta \vec{j} \sin \omega t, \tag{16}$$

where

$$U_1 = a\omega \frac{h_2(\rho_1 - \rho_2)}{h_1\rho_2 + h_2\rho_1} = a\widetilde{U}_1 \quad \text{and} \quad U_2 = -a\omega \frac{h_1(\rho_1 - \rho_2)}{h_1\rho_2 + h_2\rho_1} = a\widetilde{U}_2. \tag{17}$$

The corresponding pressure field is given by the expression

$$p_\beta = -\rho_\beta g z + a\omega^2 \rho_1 \rho_2 \frac{h_1 + h_2}{h_1\rho_2 + h_2\rho_1} x \cos \omega t. \tag{18}$$

The above solution corresponds to a plane-parallel, unsteady, counter flow which keeps the interface flat ($\xi = 0$). Note that in the case of equal densities, $\vec{V}_1$ and $\vec{V}_2$ tend to zero, i.e. both fluids stay at rest in the cavity frame. In the case $\rho_2 \ll \rho_1$, the lower fluid stays at rest in the laboratory frame ($U_1 = a\omega$).

Thus, in the inviscid case we deal with the stability problem for the interface between two counter flows, and the difference between the flow velocities is a periodic function of time. A similar problem was studied in [8]. Our formulation differs from it, in that we consider two layers of finite heights. This difference is significant for disturbances of wavelength comparable to the layer heights, or greater. Similarly to [8], the linear stability problem could be reduced to an ordinary differential equation for the amplitude $\xi(t)$ of the interface displacement from its quasi-equilibrium horizontal position:

$$\begin{aligned}(F_1 + F_2)\frac{d^2\xi}{dt^2} + 2ik\frac{d\xi}{dt}(F_1U_1 + F_2U_2)\sin \omega t \\ + \xi\left(\alpha k^3 + (\rho_1 - \rho_2)gk + i(F_1U_1 + F_2U_2)k\omega \cos \omega t - k^2\left(F_1U_1^2 + F_2U_2^2\right)\sin^2 \omega t\right) = 0,\end{aligned} \tag{19}$$

with $F_1 = \rho_1 \coth(kh_1)$ and $F_2 = \rho_2 \coth(kh_2)$. In (19), k is the wavenumber of the disturbances, which determines the periodicity of the solution along the vibration axis. It is straightforward to show that the stability problem admits the analogue of Squire's theorem [11]. This allows us to restrict ourselves to 2D-plane disturbances. Note that as $h_1, h_2 \to \infty$, our equation (19) transforms into the equation (3.8) of [8].

It is convenient to eliminate from (19) the term which contains the first order derivative in ξ. To do so, we make the change of variable [12]

$$\xi(t) = Y(t)e^{i\Phi(t)}, \tag{20}$$

where

$$\Phi = \frac{k}{\omega}\frac{F_1U_1 + F_2U_2}{F_1 + F_2}\cos\omega t \tag{21}$$

(since Φ is real, then ξ and Y are equal via a modulus, i.e. ξ and Y are equivalent from the point of view of stability). This results in the standard Mathieu equation for Y:

$$\frac{d^2Y}{dt^2} + \left(A - Q\cos^2 t\right)Y = 0. \tag{22}$$

The equation (22) is in dimensionless form, with the following reference quantities for time and length:

$$t^* = 1/\omega \quad \text{and} \quad l^* = l_c = \left[\alpha/\left(g(\rho_1 - \rho_2)\right)\right]^{1/2},$$

where l_c is the capillary length, and with the following notation:

$$Q = \frac{4B_v k^2}{We_1}\frac{\rho\coth(kH_1)\coth(kH_2)}{(\rho\coth(kH_1) + \coth(kH_2))^2}\frac{(H_1 + H_2)^2(\rho - 1)^2}{(H_1 + H_2\rho)^2}, \tag{23}$$

$$A = \frac{k(1 + k^2)}{We_1}\frac{\rho - 1}{\rho\coth(kH_1) + \coth(kH_2)}. \tag{24}$$

In formulas (23) and (24), $We_1 = \omega^2 l_c/g$ is the Weber number based on the capillary length, $\rho = \rho_1/\rho_2$ is the density ratio, $H_1 = h_1/l_c$ and $H_2 = h_2/l_c$ are dimensionless layer thicknesses. We also introduced the dimensionless parameter B_v, characterizing the vibration intensity:

$$B_v = \frac{a^2\omega^2}{4}\left(\frac{\rho_1 - \rho_2}{g\alpha}\right)^{1/2}.$$

The solutions of the equation (22), which correspond to the neutral boundary, form two classes: Y_+, having period 2π (harmonic disturbances) and Y_-, having period π (subharmonic disturbances). The solutions of subharmonic type are antiperiodic, that means that they change sign for a shift of π. Note that, from (20) and (21), the function $\xi_-(t)$ is not antiperiodic. For a shift equal to the vibration period, both types of solutions are invariant, and in this sense they are harmonic. For a shift of π the solutions $\xi_-(t)$ transform like $\xi_-(t + \pi) = -\xi_-^*(t)$ (if Y is chosen real, that is always possible; * stands for complex conjugate). At the same time $\xi_+(t + \pi) = \xi_+^*(t)$. The co-existence of the two classes of critical disturbances is associated with the invariance of equation (19) with respect to a shift of half a vibration period and complex conjugate.

We plot the boundaries of the instability regions (obtained by numerical integration of the Mathieu equation (22)) in terms of the two parameters, B_v and k. The neutral curves shown in *figures 2* and *3* correspond to Weber numbers to $We_1 = 10$ and $We_1 = 100$ (for $H_1 = H_2 = 1$, and $\rho = 2$) respectively.

The left curve in these figures (for $H_1 = H_2 = 1$) bounds the Kelvin–Helmholtz instability region, where the most dangerous are longwave disturbances with $k = 0$. The case $We_1 \to \infty$ with finite heights of the layers was investigated in [7]; for $H_1 = H_2$, it was found that the transition from the longwave instability to the finite wavelength instability occurs at $H_1 = H_2 = H_* = \sqrt{3}$. It is not difficult to analyse the longwave instability for

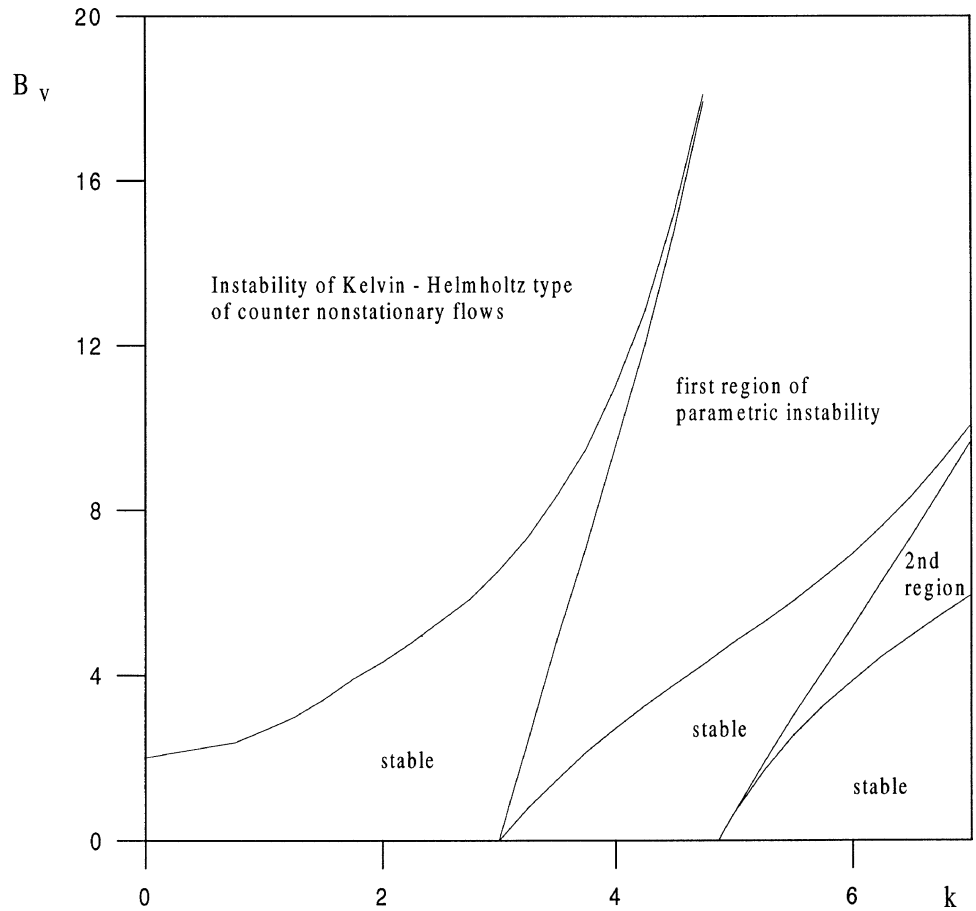

Figure 2. Neutral stability diagram (inviscid case), for $We_1 = 10$. Unstable tongues touch the k-axis at points k_n. The tongues become narrower as n increases. The tongues shift towards the shortwave region as the vibration frequency increases (see *figure 3*).

finite We_1. Indeed, for small k, Q and A are small too, and can be expanded in power series in k. The result is that for $H < H_*$ the longwave instability takes place at any values of We_1, but for $H > H_*$ it occurs only for

$$We_1 < We_{1*} = \frac{3}{8}\frac{H}{H^2-3}\,\frac{\rho-1}{\rho+1}. \tag{25}$$

For completeness, in *figures 4* and *5* we present the boundary of the primary instability region (K.H.) for different thicknesses of fluid layers. The other parameters are $\rho = 2$, $We_1 = 1$. The neutral curve shown in *figure 4* corresponds to $H = H_1 = H_2 = 2 > H_*$ and we observe finite wavelength instability, because here $We_{1*} = 0.25$ violates (25). The effect of H is shown in *figure 5* where this last result (*figure 5(a)*) is compared to the boundary curves obtained for $H = 5$ and $H = 25$ (*figures 5(b)* and *5(c)*, respectively) for which $We_{1*} = 0.028$ and 0.005, respectively; both violate (25). The present results are consistent with [8] who investigated the case $H \to \infty$ for large values of We_1. For this case (in our notation) the critical value of B_v is given by the expression

$$B_v = \frac{1+k^2}{k}\,\frac{\rho+1}{\rho(\rho-1)}. \tag{26}$$

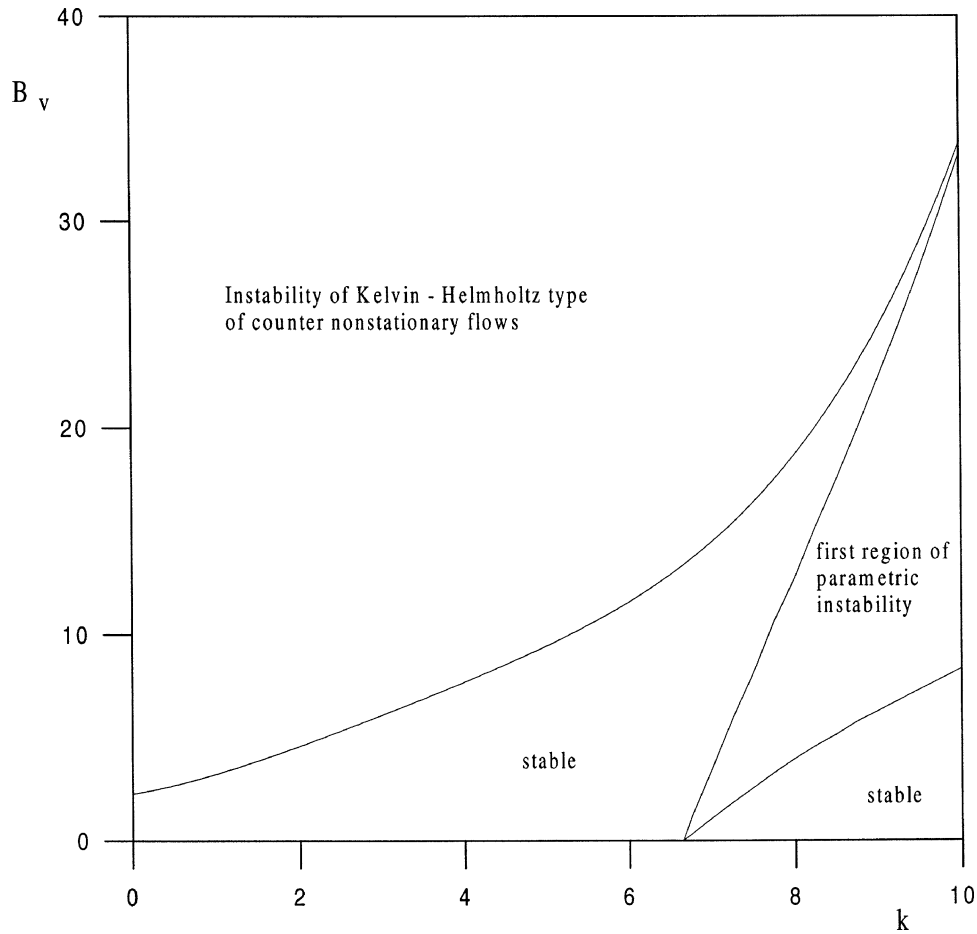

Figure 3. Neutral stability diagram (inviscid case), for $We_1 = 100$. The comparison of this and *figure 2* reveals that the influence of changes in the vibration frequency on Kelvin–Helmholtz instability is very small.

This instability mechanism is, in fact, the same as in the standard case of Kelvin–Helmholtz instability: the velocity grows and the pressure falls over the elevations of the interface. The consequence of this is the reduction of the effective stiffness of the system and the rise of the instability beyond some threshold. As shown in [7], in the case of high frequency vibration, the nonlinear development of such an instability results in the formation of a quasi-stationary wave relief on the interface.

However, periodic changes of the velocity can result not only in the average effect, but in the resonance amplification of eigen-oscillations. In the absence of dissipation, the eigen-oscillations are not damped, and the instability will occur at an infinitely small vibration amplitude (if the synchronism condition is satisfied). In *figures 2* and *3* the regions of parametric instability approach the abscissa as narrow ends ('tongues'); the points k_n at which the n-th region of instability is in contact with the k-axis can be evaluated from the equation $A = n^2,\ n = 1, 2, \ldots$. In the case $h \to \infty$, these points and the boundaries of instability regions in their vicinity were found in [8]. As the vibration frequency grows, i.e. as the Weber number increases, the points k_n shift to the shortwave region (as seen from *figures 2* and *3*) and in the limiting case $We_1 \to \infty$, they are displaced to infinity. Thus, for high frequency vibrations the parametric instability can take place only for shortwave disturbances; then, the viscosity cannot be ignored. For large values of the Weber number only the quasi-static instability must be observed, with an excitation mechanism which is weakly sensitive to the viscosity.

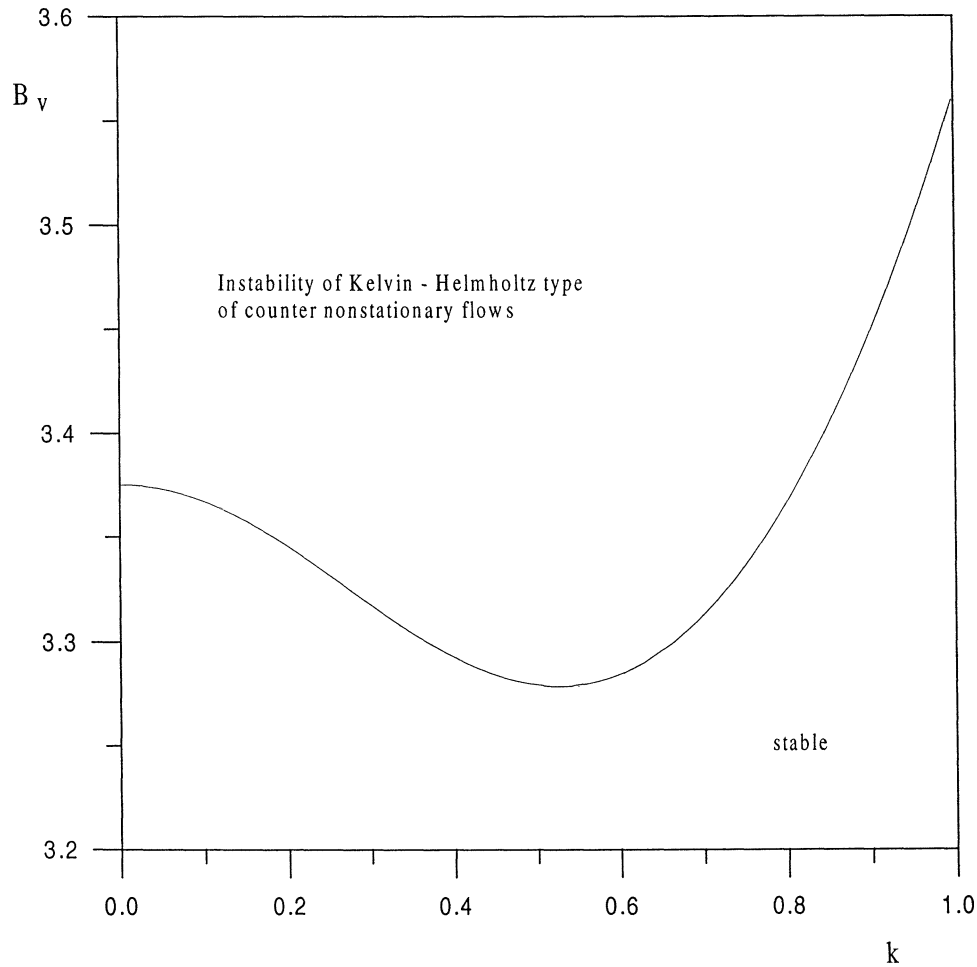

Figure 4. Boundary of primary instability region (inviscid case), for $\rho = 2$, $We_1 = 1$, $H = 2 > H_*$ and $We_{1*} = 0.25 < We_1$. Finite wavelength instability is observed, in contrast to *figures 2* and *3*.

4. 2D linear stability problem for viscous fluids

To simplify the presentation, we assume in this section that the two layers are of equal height $h_1 = h_2 = h$. In addition, we non-dimensionalize the problem by using the scaling factor:

$$t^* = 1/\omega, \qquad l^* = h, \qquad u^* = a\omega, \qquad p^* = \rho_2 ha\omega^2.$$

4.1. Problem formulation

The following dimensionless equations replace equations (2)–(8):

$$\frac{\partial \vec{v}_\beta}{\partial t} + A(\vec{v}_\beta \nabla)\vec{v}_\beta = -R_\beta \nabla p_\beta + \Omega_\beta^{-1} \Delta \vec{v}_\beta - G_0 A^{-1} \vec{\gamma} + \vec{k} \cos t, \tag{27}$$

$$\operatorname{div} \vec{v}_\beta = 0, \tag{28}$$

$$\text{at } z = -1: \quad \vec{v}_1 = 0, \tag{29}$$

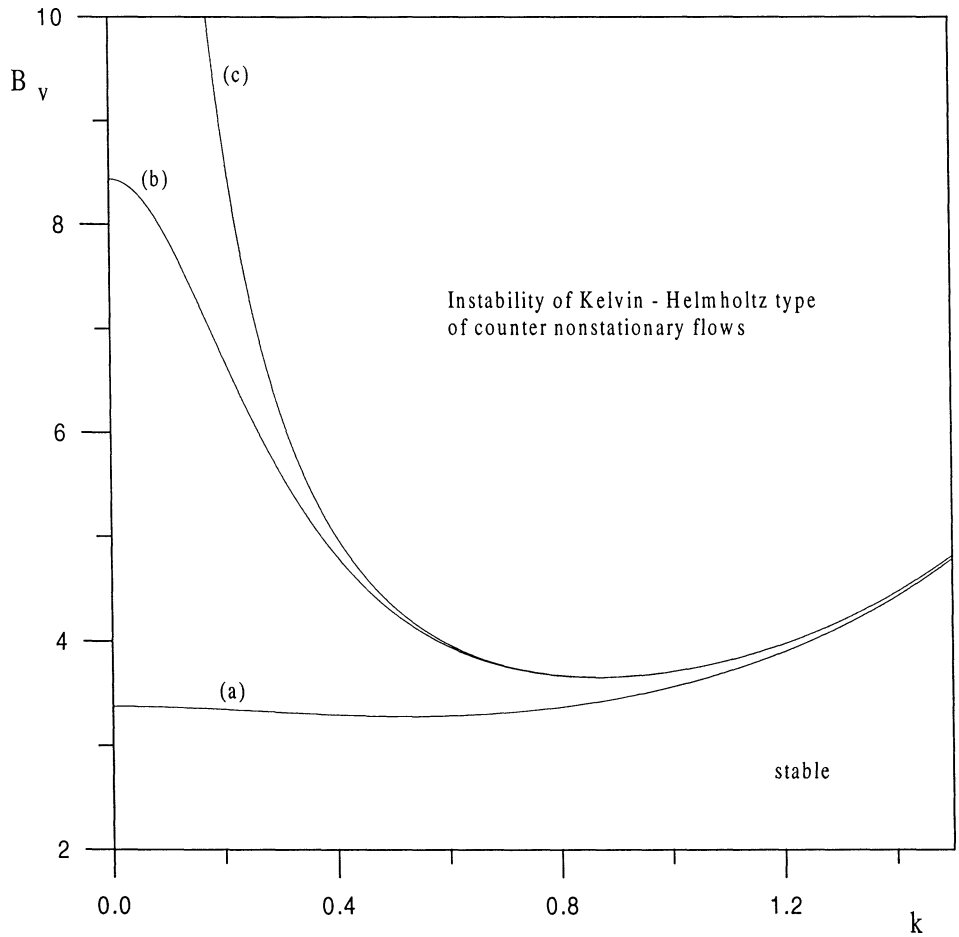

Figure 5. Boundary of primary instability region (inviscid case), for $\rho = 2$, $We_1 = 1$: (a) $H = 2 > H_*$ and $We_{1*} = 0.25 < We_1$; (b) $H = 5 > H_*$ and $We_{1*} = 0.028 < We_1$; (c) $H = 25 > H_*$ and $We_{1*} = 0.005 < We_1$.

$$\text{at } z = 1: \quad \vec{v}_2 = 0, \tag{30}$$

$$\text{at } z = \xi(x, y, t): \quad [p]n_i = (\Omega_1^{-1}\rho\sigma_{ik}^{(1)} - \Omega_2^{-1}\sigma_{ik}^{(2)})n_k + A^{-1}We_2^{-1}n_i \operatorname{div}\vec{n}, \tag{31}$$

$$[\vec{v}] = 0, \tag{32}$$

$$\frac{1}{A}\frac{\partial\xi}{\partial t} + (\vec{v}_1\nabla)\xi = \vec{v}_1 \cdot \vec{\gamma}, \tag{33}$$

$$\forall x: \quad \int_{-1}^{\xi} \vec{v}_1 \cdot \vec{j}\, dz + \int_{\xi}^{1} \vec{v}_2 \cdot \vec{j}\, dz = 0. \tag{34}$$

Here and below, the quantity jump across the interface is denoted by square brackets, for example $[p] = p_1 - p_2$, and the following parameters are introduced: $A = ah^{-1}$, dimensionless amplitude; $\Omega_1 = h^2\omega\nu_1^{-1}$ and $\Omega_2 = h^2\omega\nu_2^{-1}$, dimensionless frequencies; $G_0 = g/(h\omega^2)$; $We_2 = \rho_2 h^3\omega^2/\alpha$, a new Weber number; $\rho = \rho_1/\rho_2$, the density ratio; $R_1 = 1/\rho$ and $R_2 = 1$.

So, the system of governing equations contains 7 dimensionless parameters: A, Ω_1, Ω_2, G_0, We_2, ρ and the wave number k.

4.2. Solution method

The system of equations (27)–(34) admits a solution of the form

$$\vec{V}_\beta = U_\beta(z)\vec{j}\exp(it) + \text{C.C.}, \tag{35}$$

$$P_\beta = -G_0 A^{-1} R_\beta^{-1} z + x\big(S\exp(it) + \text{C.C.}\big), \quad S = \text{const}. \tag{36}$$

The above solution corresponds to the plane-parallel unsteady counter flow which keeps the interface flat ($\xi = 0$) (to be compared with (16)–(18) in the inviscid case). The function $U_\beta(z)$ could be found analytically, but its expression is too complicated, so it was determined numerically. *Figure 6* represents the velocity profiles at four time instants: (a) $t = 0$, (b) $t = \pi/2$, (c) $t = \pi$, (d) $t = 3\pi/2$. The direction of the flow changes every half period of the external forcing. Note the thin boundary layers at both sides of the interface and near the walls (*figures 6(a)* and *6(c)*).

For the reasons discussed in Section 3, we investigate the stability of the basic state (35), (36) with respect to periodic (in time and space) 2D disturbances. If the vibration frequency is high enough, then thin boundary layers occur at the interface (on both sides) and near the two horizontal walls, making the task of numerical solution particularly complicated.

After linearizing near the solution (35) and (36), the Navier–Stokes equations for small disturbances $\vec{u}_\beta$ and p_β are

$$\frac{\partial \vec{u}_\beta}{\partial t} + A(\vec{V}_\beta\nabla)\vec{u}_\beta + A(\vec{u}_\beta\nabla)\vec{V}_\beta = -R_\beta\nabla p_\beta + \Omega_\beta^{-1}\triangle\vec{u}_\beta, \tag{37}$$

$$\operatorname{div}\vec{u}_\beta = 0. \tag{38}$$

The boundary conditions for the system (37)–(38) becomes

$$\text{at } z = -1: \quad \vec{u}_1 = 0, \tag{39}$$

$$\text{at } z = 1: \quad \vec{u}_2 = 0, \tag{40}$$

$$\text{at } z = 0: \quad A^{-1}\big((1-\rho)G_0\xi + We_2^{-1}\Delta\xi\big)n_i + [p]n_i = \big(\Omega_1^{-1}\rho\sigma_{ik}^{(1)} - \Omega_2^{-1}\sigma_{ik}^{(2)}\big)n_k, \tag{41}$$

$$[\vec{u}] = -\left[\frac{\partial\vec{V}}{\partial z}\right]\xi, \tag{42}$$

$$\frac{1}{A}\frac{\partial\xi}{\partial t} + (\vec{V}_1\nabla)\xi = u_{1z}. \tag{43}$$

This is valid as long as the deformation ξ is small compared to the wavelength of the instability.

It is easy to see that the problem is uniform in the x-direction. This allows us to consider only normal disturbances. The linear stability problem is now summarized as

$$\frac{\partial u_\beta}{\partial t} + ikAV_\beta u_\beta + w_\beta A\frac{\partial V_\beta}{\partial z} = -ikR_\beta p_\beta + \Omega_\beta^{-1}\left(\frac{\partial^2}{\partial z^2} - k^2\right)u_\beta, \tag{44}$$

$$\frac{\partial w_\beta}{\partial t} + ikAV_\beta w_\beta = -R_\beta\frac{\partial p_\beta}{\partial z} + \Omega_\beta^{-1}\left(\frac{\partial^2}{\partial z^2} - k^2\right)w_\beta, \tag{45}$$

$$iku_\beta + \frac{\partial w_\beta}{\partial z} = 0, \tag{46}$$

$$\text{at } z = -1: \quad u_1 = w_1 = 0, \tag{47}$$

$$\text{at } z = 1: \quad u_2 = w_2 = 0, \tag{48}$$

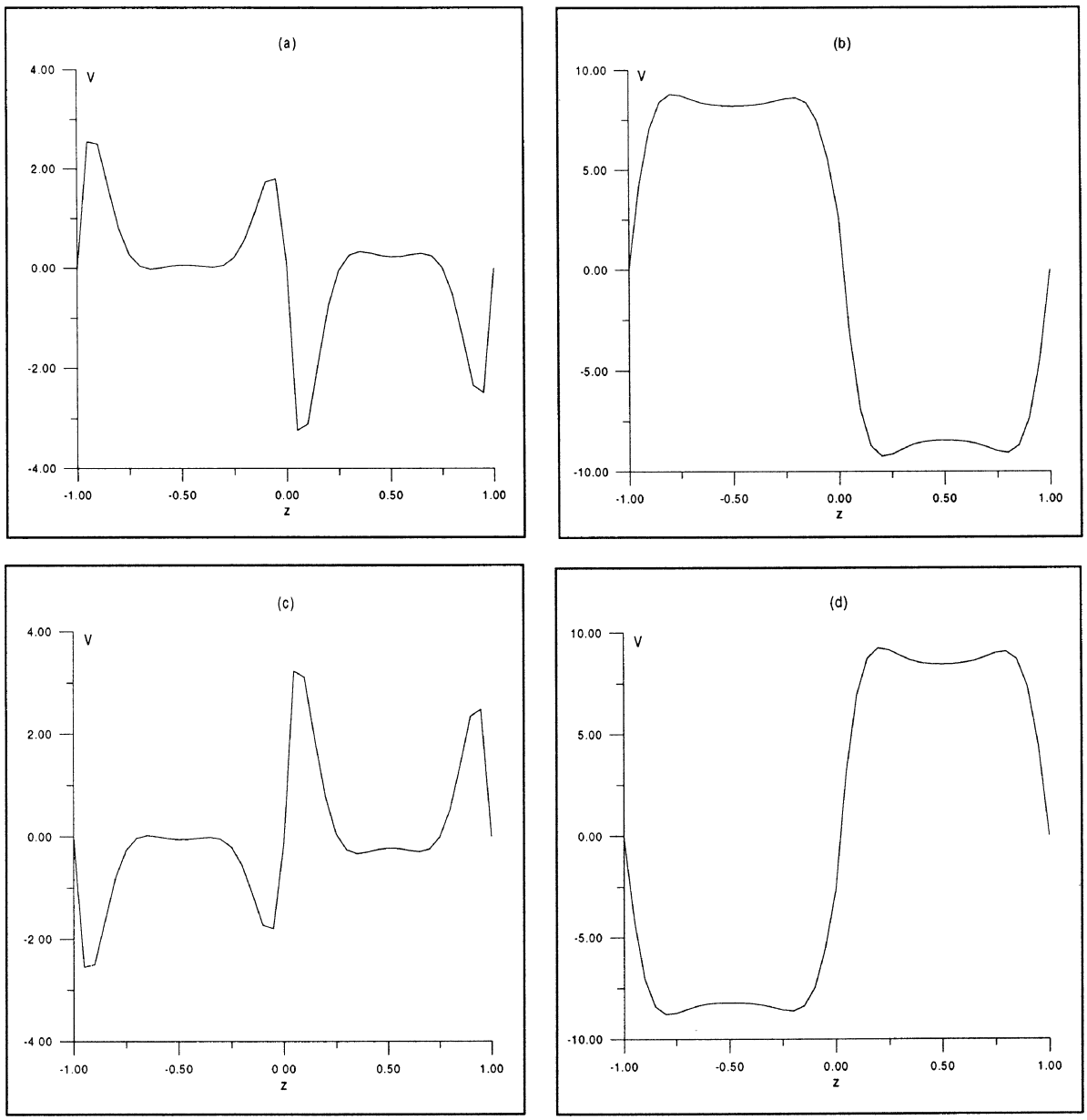

Figure 6. Velocity profile at four time instants (viscous case): (a) $t = 0$, (b) $t = \pi/2$, (c) $t = \pi$, (d) $t = 3\pi/2$. Flow direction changes every half period of the forcing vibration. Note thin boundary layers at both sides of the interface and near the walls (*figures 6(a)* and *6(c)*).

$$\text{at } z = 0: \qquad A^{-1}\xi\left((1-\rho)G_0 - We_2^{-1}k^2\right) + [p] + 2\left(\Omega_2^{-1}\frac{\partial w_2}{\partial z} - \Omega_1^{-1}\rho\,\frac{\partial w_1}{\partial z}\right) = 0, \tag{49}$$

$$-\frac{\Omega_2}{\Omega_1}\rho\left(ikw_1 + \frac{\partial u_1}{\partial z} + \xi\frac{\partial^2 V_1}{\partial z^2}\right) + ikw_2 + \frac{\partial u_2}{\partial z} + \xi\frac{\partial^2 V_2}{\partial z^2} = 0, \tag{50}$$

$$[u] = -\left[\frac{\partial V}{\partial z}\right]\xi, \tag{51}$$

$$[w] = 0, \tag{52}$$

$$\frac{1}{A}\frac{\partial \xi}{\partial t} + ikV_1\xi = w_1. \tag{53}$$

All fields could be expanded in time in Fourier series of the form

$$f_\beta(z,t) = \sum_{n=-\infty}^{\infty} f_{n\beta}(z)\exp(int) + \text{C.C.},$$

where n might be taken integer, as well as half-integer. By keeping only a finite number of terms of the expansion in both fluids, we get 2-point boundary value problems (BVP's, coupled through the conditions (49)–(53)), for the system of ordinary differential equations for the complex amplitudes $p_{n\beta}(z)$, $u_{n\beta}(z)$, $w_{n\beta}(z)$ (note that $\xi_n(z)$ may be eliminated from (49)–(53)). The coefficients in the equations depend on z, therefore the system could only be resolved numerically.

One important feature of the resulting ODE's systems is that integer and half-integer harmonics are not coupled (since the basic flow (35) introduce only a shift of ± 1 for n in (44)–(53)). Thus, the corresponding BVP's can be solved independently. The solutions of the BVP's involving integer harmonics have the same period as that of the forcing vibration (harmonic, or synchronous case) and the solutions of the BVP's involving half-integer harmonics have a period twice as that of the forcing vibration (subharmonic, or asynchronous case).

BVP's, in turn, allow the reduction to initial values problems (IVP's). We focus our attention on the synchronous case, since asynchronous solutions were not detected in the numerical investigation. The numerical procedure is described in [13], so we give only a brief description.

Let N be the number of integer harmonics retained. In order to obtain the numerical solution to the problem in the synchronous case, a system of $4N$ first order ODE's in each fluid has to be integrated $2N$ times from the wall to the interface (we use the routine LSODA from the collection of ODE solvers ODEPACK, based on Adams predictor–corrector method [14,15]), each time with a different set of initial conditions. These sets of initial conditions are chosen linearly independent. Some of the initial conditions, forming a particular set, satisfy the no-slip conditions on rigid walls, the others are chosen in such a way to preserve the linear independence of the set. Let us denote the vectors of the particular solutions obtained by the integration as $\mathbf{y}^{(i)}$, $i = 1, 2, \ldots, 2N$. Then the general solution is $\mathbf{y} = C_1\mathbf{y}^{(1)} + C_2\mathbf{y}^{(2)} + \cdots + C_{2N}\mathbf{y}^{(2N)}$. The substitution of $\mathbf{y}$ into interface conditions (49)–(53) results in a system of homogeneous algebraic equations for the unknown coefficients C_i. The condition of the existence of a non-trivial solution to this system is $D = 0$, D being a determinant. D is (as well) a function of the wavenumber k and the dimensionless amplitude A. The value $A = A_c$ at which D becomes zero (for fixed k) is the critical value. So for $N = 10$ (which is sufficient in most cases), the 40 ODE's must be integrated $(2 * 10) * 2 = 40$ times to obtain the single value of D, for fixed k and A. This procedure must be repeated several times to get $D = 0$ at $A = A_c$. For solving the algebraic equation $D(A, k, \text{other parameters}) = 0$, one can use a bisection technique or any other more efficient solver.

The alternative methodology would be to provide a matrix formulation for the above linear stability problem followed by numerical solution of the eigenvalue problem (within the framework of the Tau–Chebyshev procedure, for example). The Tau–Chebyshev method is faster than direct integration of ODE's, and yields the entire spectra of neutral curves (for fixed values of dimensionless parameters) in a single program run, while in our method each curve must be traced separately. The applicability of Tau–Chebyshev method to this problem is now under investigation.

5. Numerical results

The linear stability of the flat interface has been calculated using 21 basis functions $f_n(z)$ in both cases (synchronous and asynchronous). Ten to twelve basis functions are enough to get sufficiently accurate numerical results if the dimensionless frequency is not high ($\Omega \lessapprox 250$). The number of basis functions must be increased if $\Omega > 250$. In addition, at high values of Ω, the linear independence of the particular solutions is lost in the integration process, resulting in an ill-conditioned coefficient matrix of the algebraic system. At the preassigned mesh points, linear independence can be restored by means of Gram–Schmidt orthogonalization.

In *figure 7*, in addition to the boundary of the Kelvin–Helmholtz type instability, we show the neutral stability curves which divide the (k, A)-plane into regions of stable solutions, and regions (tongues) of unstable solutions (exponentially growing in time). The values of the nondimensional parameters are $\rho = 2$, $G_0 = 0.16$ and $We_2 = 6.25$. Only synchronous solutions were detected. This situation is not unique (for review and discussion, see [16]). The boundaries of the inviscid problem are plotted with solid lines, while the curves obtained numerically for viscous fluids at different values of the dimensionless frequency $\Omega_1 = \Omega_2 = \Omega$, are plotted with dashed lines (note that $\Omega_1 = \Omega_2$ correspond to $\nu_1 = \nu_2$). For the high values of Ω (i.e. for small viscosity),

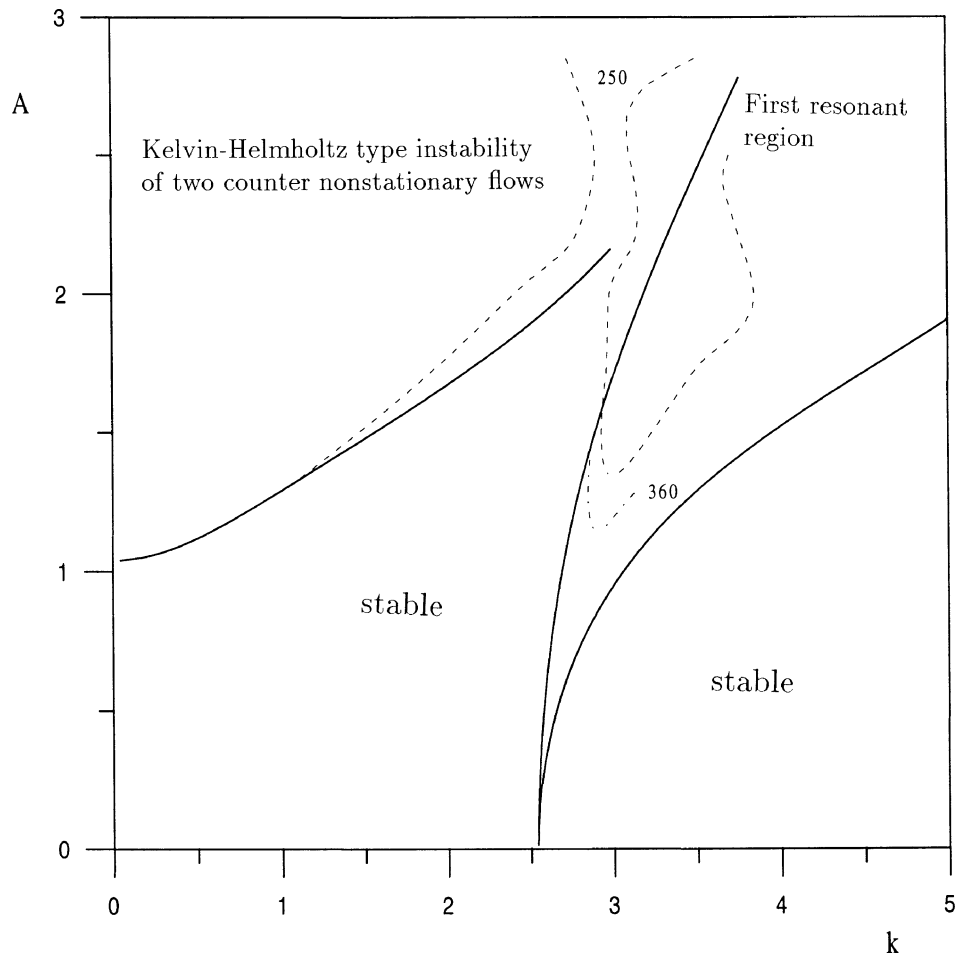

Figure 7. Neutral stability diagram k–A (viscous case); for $\rho = 2$, $G_0 = 0.16$ and $We_2 = 6.25$; for large Ω (250, 360), i.e. small viscosity.

the minimum of the numerical curve corresponding to the first region of the parametric instability approaches the bottom of the inviscid tongue (*figure 7*).

Inversely, as Ω decreases (viscosity increases), this instability threshold (of the first region of parametric instability) grows. Then, the boundary of the Kelvin–Helmholtz instability region unites with the boundary of the first resonant zone (at some Ω value between 100 and 250), so that at smaller Ω there exists a single neutral curve corresponding to each value of Ω. This means that in the case of rather viscous fluids the difference between the parametric and non-parametric instabilities vanishes (*figure 8*).

From *figures 7* and *8*, we can conclude that viscosity has a weak influence on the Kelvin–Helmholtz instability, but strongly damps the parametric instability associated with the excitation of capillary-gravity waves.

Figures 9(a) and *9(b)* represent the dependence of the instability threshold in the first resonant region, k_c and A_c, respectively, on the dimensionless frequency Ω. As the vibration frequency grows, the critical amplitude decreases and the unstable tongue is displaced into the shortwave region (compared to *figures 2* and *3*), with a good agreement with the inviscid approximation.

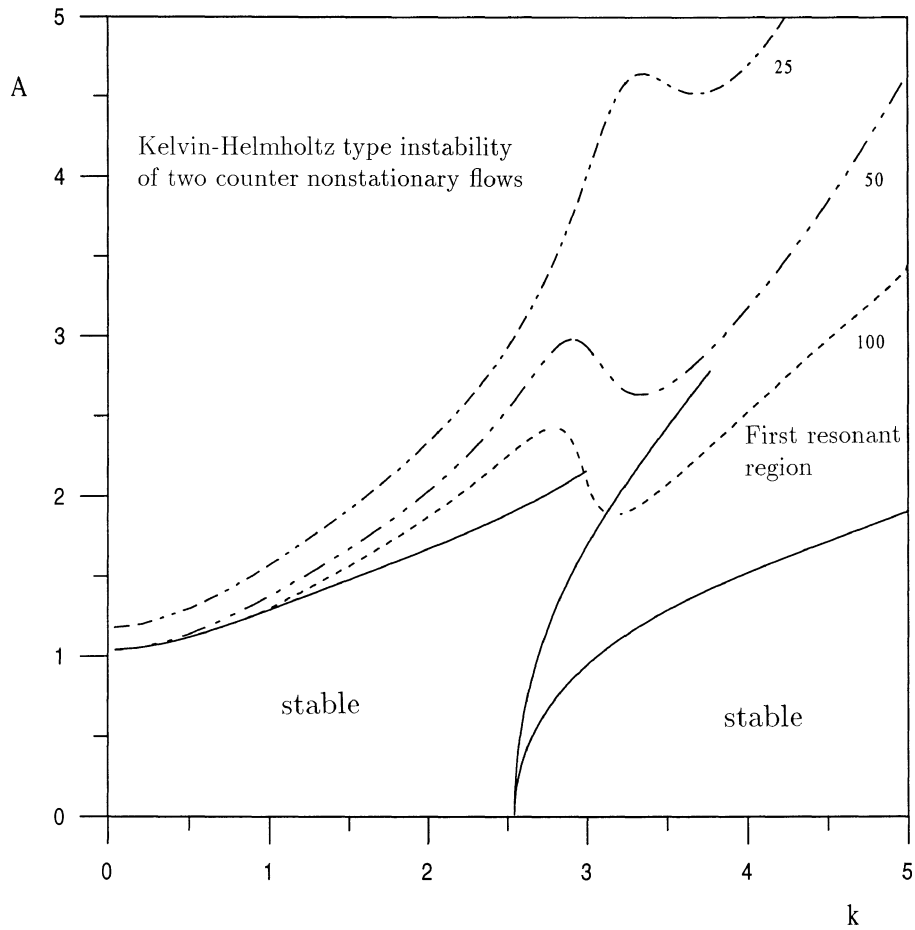

Figure 8. Neutral stability diagram k–A (viscous case); same parameters as in *figure 7*; for small Ω (25, 50, 100), i.e. large viscosity. Viscosity has a weak influence on Kelvin–Helmholtz type instability but strongly damps the parametric instability. In the case of rather viscous fluids, the difference between the parametric and non-parametric instabilities vanishes.

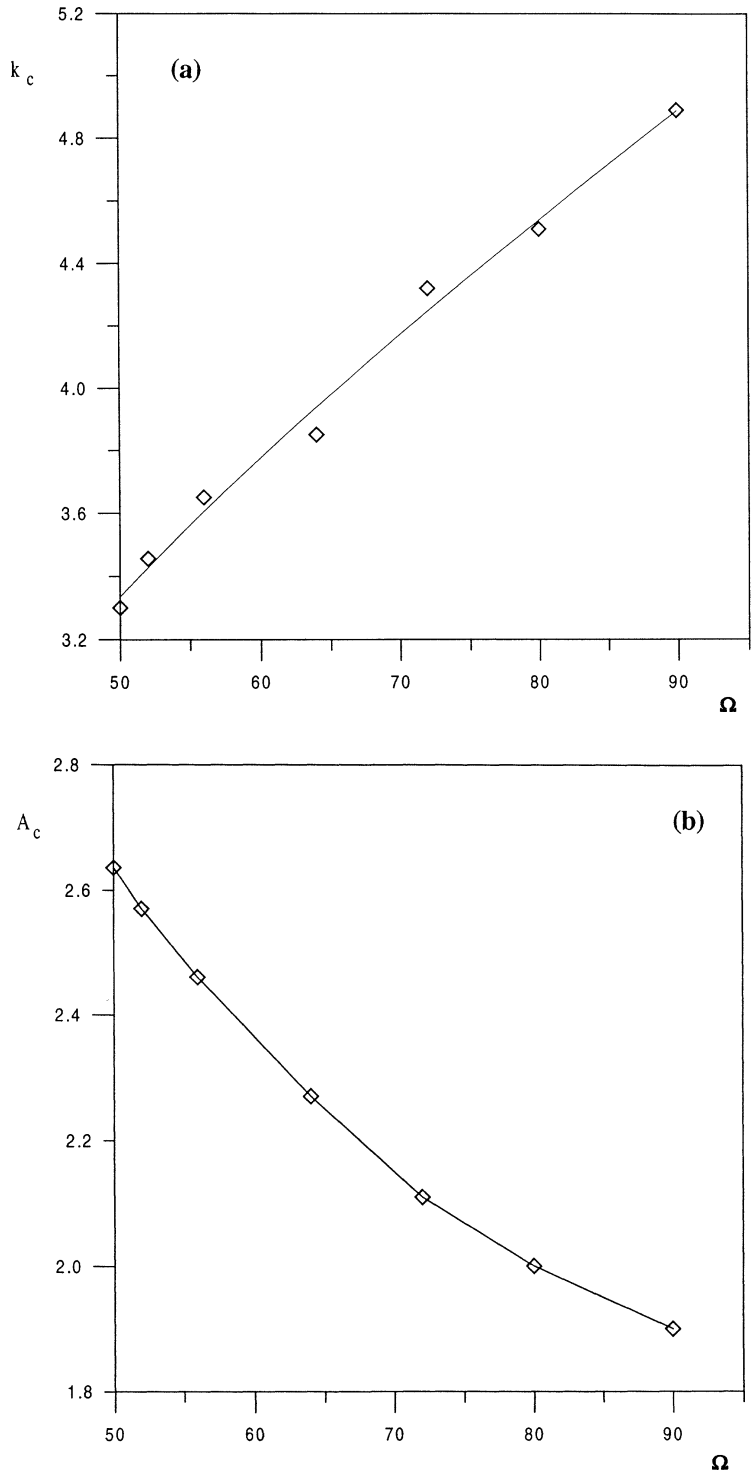

Figure 9. Instability threshold k_c and A_c as a function of Ω, in the first resonant region (viscous case); parameters are the same as in *figure 7*. (a) k_c–Ω diagram; (b) A_c–Ω diagram.

Acknowledgements

The authors wish to acknowledge the financial support of the Ministère de l'Education Nationale, de la Recherche et de la Technologie (Délégation aux Affaires Internationales; Réseau Formation–Recherche Franco–Russe) and of the Centre National d'Etudes Spatiales (CNES/DP/E2U; Division Microgravité). They also wish to warmly thank the referees for asking very pertinent questions and mentioning interesting references, and for improving the English translation of the manuscript. The computations were carried out on Silicon Graphics's Power Challenge computer of IRPHE-IMT.

References

[1] Benjamin T.B., Ursell F., The stability of a plane free surface of a liquid in vertical periodic motion, P. Roy. Soc. Lond. A 225 (1954) 505–515.
[2] Brand R.P., Nyborg W.L., Parametrically excited surface waves, J. Acoust. Soc. Am. 37 (3) (1965) 509–515.
[3] Kumar K., Tuckerman L.S., Parametric instability of the interface between two fluids, J. Fluid Mech. 279 (1994) 49–68.
[4] Wolf G.H., Dynamic stabilization of the interchange instability of a liquid–gas interface, Phys. Rev. Lett. 24 (9) (1970) 444–446.
[5] Wolf G.H., The dynamic stabilization of the Rayleigh–Taylor instability and the corresponding dynamic equilibrium, Z. Physik B. Con. Mat. 227 (3) (1969) 291–300.
[6] Bezdenezhnykh N.A., Briskman V.A., Lyubimov D.V., Cherepanov A.A., Sharov M.T., Control of the fluid interface stability by vibration, electric and magnetic fields, in: III All-Union Seminar on Hydromechanics and Heat/Mass Transfer in Microgravity, Chernogolovka, 1984, pp. 18–20 (in Russian).
[7] Lyubimov D.V., Cherepanov A.A., Development of a steady relief at the interface of fluids in a vibrational field, Fluid Dyn. Res. 22 (1987) 849–854.
[8] Kelly R.E., The stability of an unsteady Kelvin–Helmholtz flow, J. Fluid Mech. 22 (3) (1965) 547–560.
[9] Ockendon J.R., Ockendon H., Resonant surface waves, J. Fluid Mech. 59 (1973) 397–413.
[10] Ockendon J.R., Ockendon H., Multi-mode resonance in fluids, J. Fluid Mech. 315 (1996) 317–344.
[11] Squire H.B., On the stability for three-dimensional disturbances of viscous fluid flow between parallel walls, P. Roy. Soc. Lond. A 142 947 (1933) 621.
[12] Lyubimov D.V., Khenner M.V., Shotz M.M., Stability of a fluid interface under tangential vibrations, Fluid Dyn. Res. 33 (3) (1998) 318–323.
[13] Gershuni G.Z., Zhukhovitsky E.M., Convective Stability of Incompressible Fluid, Nauka, Moscow (1972) p. 392 (in Russian).
[14] Hindmarsh A.C., Odepack, a systematized collection of ode solvers, in: Stepleman R.S. et al. (Eds), Scientific Computing, North-Holland, Amsterdam, 1983, pp. 55–64.
[15] Petzold L.R., Automatic selection of methods for solving stiff and nonstiff systems of ordinary differential equations, SIAM J. Sci. Stat. Comput. 4 (1983) 136–148.
[16] Or A.C., Finite-wavelength instability in a horizontal liquid layer on an oscillating plane, J. Fluid Mech. 335 (1997) 213–232.